Title

Structural Basis for a Species-Specific Determinant of an SIV Vif Protein toward Hominid APOBEC3G Antagonism

Authors

Binning, Jennifer M
Chesarino, Nicholas M
Emerman, Michael
et al.

Structural basis for a species-specific determinant of an SIV Vif protein towards hominid APOBEC3G antagonism

Jennifer M. Binning[1], **Nicholas M. Chesarino**[2], **Michael Emerman**[2,*], **John D. Gross**[1,3,*]

[1]Department of Pharmaceutical Chemistry, University of California, San Francisco, California 94158, USA.

[2]Divisions of Human Biology and Basic Sciences, Fred Hutchinson Cancer Research Center, Seattle, Washington 98109, USA

[3]Lead Contact

Summary

Primate lentiviruses encode a Vif protein that counteracts the host antiviral APOBEC3 (A3) family members. The adaptation of Vif to species-specific A3 determinants is a critical event that allowed the spillover of a lentivirus from monkey reservoirs to chimpanzees and subsequently to humans, which gave rise to HIV-1 and the AIDS pandemic. How Vif-A3 protein interactions are remodeled during evolution is unclear. Here, we report a 2.94 Å crystal structure of the Vif substrate receptor complex from simian immunodeficiency virus isolated from red-capped mangabey (SIVrcm). The structure of the SIVrcm Vif complex illuminates the stage of lentiviral Vif evolution immediately prior to entering hominid primates. Structure-function studies reveal the adaptations that allowed SIVrcm Vif to antagonize hominid A3G. These studies show a partitioning between an evolutionarily dynamic specificity determinant and a conserved protein interacting surface on Vif that enables adaptation while maintaining protein interactions required for potent A3 antagonism.

eTOC Blurb

Lentiviral transmission from Old World monkeys to hominid primates require adaptations of viral Vif to hominid APOBEC3s. Binning et al. present the crystal structure of the SIVrcm Vif complex, providing insight into evolutionary requirements for cross-species transmission of SIV into hominid primates that underlie the origins of HIV-1 in humans.
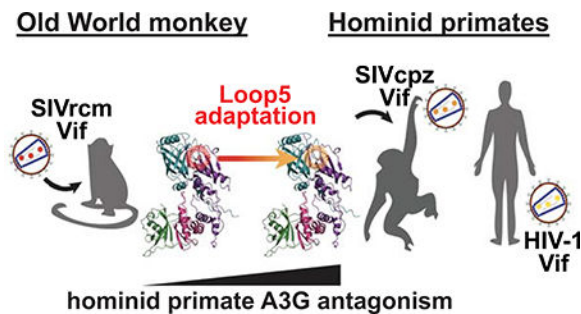
Graphical Abstract

Introduction

The HIV-1 pandemic is the end result of a series of recombination and zoonotic transmission events among primate lentiviruses. The HIV-1 precursor, Simian Immunodeficiency Virus from chimpanzees (SIVcpz), originated from the recombination of at least two Old World monkey SIV strains. Subsequently, cross-species transmission of SIVcpz from chimpanzees into humans ultimately led to the emergence of HIV-1 (Bailes et al., 2003; Sharp and Hahn, 2011). Evolutionary pressures placed upon lentiviruses such as SIV/HIV and their affected hosts have resulted in a molecular "arms race" which has shaped both host immunity and pathogen immune evasion strategies (Daugherty and Malik, 2012). Central to this race is the lentiviral protein Vif, encoded by nearly all existing lentiviruses (Gifford, 2012) and essential for replication *in vivo* (Desrosiers et al., 1998).

The primary function of Vif is to counteract the antiviral effects of host APOBEC3 (A3) proteins, a family of restriction factors that function by hypermutating viral genomes (Harris and Dudley, 2015). Vif employs multiple strategies to counteract A3 proteins (Anderson and Harris, 2015; Binning et al., 2018; Kim et al., 2013); but the most well-established mechanism involves hijacking of a cellular Cullin-RING ubiquitin ligase, resulting in the ubiquitination and subsequent targeting of A3 for proteasomal degradation (Hultquist et al., 2011; Sheehy et al., 2002; Yu et al., 2003). HIV-1 Vif is able to antagonize multiple A3 proteins, including APOBEC3F (A3F), APOBEC3C (A3C), APOBEC3D (A3D), APOBEC3G (A3G), and APOBEC3H (A3H). However, the interaction between Vif and the A3 proteins is often species-specific, and compensatory mutations among viral *vif* and host *A3* genes are key determinants of interspecies transmission events such as the zoonotic transmission events that resulted in SIVcpz and HIV-1 (Compton et al., 2013).

The SIVcpz *vif* gene is derived from an ancestral virus related to the lentivirus that currently infects the red-capped mangabey (SIVrcm). During the genesis of SIVcpz from SIVrcm, a gene encoding the protein Vpx was deleted which caused an overprinting of *vif* into the *vpr* open reading frame creating a new C-terminus of Vif (Etienne et al., 2013). The resulting Vif acquired the ability to antagonize chimpanzee A3G and A3D, and the Vif adaptation from red-capped mangabey to chimpanzees was a major event in overcoming species-specific barriers imposed by hominid primate A3s. A critical but unresolved question is how adaptations in *vif* manifest as structural and biophysical changes that allow it to neutralize restrictive APOBEC3 family members during cross-species transmission.

HIV-1 Vif can counteract human A3G (huA3G), but not African green monkey (agm) A3G, and vice versa; however, if residue 128 in huA3G is mutated from an aspartic acid to a lysine (D128K), HIV-1 Vif loses the ability to antagonize this A3G mutant and SIVagm Vif gains the ability to degrade it (Bogerd et al., 2004; Schröfelbauer et al., 2004; Xu et al., 2004). Likewise, despite its essential role in SIVrcm infection, the SIVrcm Vif protein is a poor antagonist of chimpanzee A3D and A3G proteins (Etienne et al., 2013, 2015) which would be essential for the cross-species transmission of SIV from old world monkeys into chimpanzees. In an effort to rationalize a structural mechanism for species-specific A3 recognition, we sought to determine adaptations that were required for SIVrcm to adapt to antagonize chimpanzee A3s.

Here we present the structure of the substrate receptor complex of the Vif ubiquitin ligase, consisting of SIVrcm <u>V</u>if, <u>C</u>BFβ, ELONGIN <u>B</u> (ELOB), and ELONGIN <u>C</u> (ELOC) (termed VCBC) (Figure 1A) (Guo et al., 2014; Jäger et al., 2011; Zhang et al., 2012; Zhou et al., 2012). The SIVrcm VCBC structure provides a "snapshot" of Vif at the stage of lentiviral evolution immediately prior to entering hominid primates. By combining the structural insight gained from the SIVrcm VCBC structure with functional viral infectivity studies, we have determined viral adaptations that arose during the cross-species transmission from Old World monkeys (OWMs) to chimpanzees that enabled SIVrcm Vif to efficiently antagonize chimpanzee A3G (cpzA3G).

Results

Crystal structure of the SIVrcm A3 substrate receptor complex

To determine how Vif adaptations that arose during the cross-species transmission event from OWM to hominid primates allowed antagonism of A3 restriction factors, we solved the crystal structure of SIVrcm VCBC complex to 2.94Å (Figure 1A, Figure 1B, and Table 1). To generate this complex, we use human co-factors CBFβ, ELOB, and ELOC as previous studies have shown that primate Vifs, including SIVrcm Vif, expressed in human cells can use these proteins to assemble in a fully functional E3 ligase and antagonize their cognate APOBEC3s (Compton and Emerman, 2013; Compton et al., 2012; Etienne et al., 2013, 2015). A comparison of the SIVrcm Vif and HIV-1 Vif structures revealed that the overall protein fold is the same, but the length of C-terminal loops vary significantly between the structures, which precluded construction of reliable homology models (Figures 1B and S1) (Guo et al., 2014). Notable similarities between the HIV-1 and SIVrcm Vif complex structures include (1) the large domain (a/p domain) of SIVrcm Vif interacts with CBFβ through an extended, antiparallel β-sheet; (2) The small domain (a domain) of SIVrcm Vif is formed by two loosely packed helixes that contain the conserved BC-box motif that is responsible for engaging the ELOBC subunits; and (3) HIV-1 Vif and SIVrcm Vif coordinates a Zn^{2+} through their zinc-finger motif, HCCH, and this, in turn, stabilizes the three inter-domain loops.

Despite the similarities in the protein fold of SIVrcm and HIV-1 Vifs, a detailed comparison of the two structures reveals several differences. Alignment of HIV-1 Vif with SIVrcm Vif shows that the length of the BC-box containing helix differs between SIVrcm and HIV-1 Vif. The BC-box containing helix (a4), which is responsible for binding to ELOBC, makes

an additional turn in the SIVrcm Vif structure (Figure 1C). Within the overprinted region of Vif, the position of secondary structured elements is the same but loops preceding and following α5 are different both in amino acid identity and length (Figure 1C, Figure S1). Specifically, the repositioning of α5 in the primary sequence results in HIV-1 Vif having approximately 20 amino acids following α5 that are absent in SIVrcm Vif, and SIVrcm Vif having an extended, flexible linker of 47 residues (as compared to 11 residues in HIV-1) separating the BC-box from α5 (Figures S1 and S2). Of note, this region of HIV-1 Vif contains critical A3 binding residues and the acquired PPLP motif that are both absent in SIVrcm Vif (Etienne et al., 2013).

In addition to the changes in the overprinted region of Vif, there are also differences that affect the conformation and charge of the VCBC complexes. Alignment of the ELOBC subunits from the two VCBC complexes shows a rotational change in Vif that results in a displacement of CBFβ between the two structures (Figure 1D). It is unclear if this difference is caused by HIV-1 VCBC being bound to CUL5ntd in the HIV-1 structure or differences in crystal packing; however, previous NMR and negative stain EM studies of VCBC complexes have shown Vif to be flexible as the large and small domains of Vif can move relative to each other, likely through hinge-like movements at the inter-domain loop region (Ball et al., 2018; Binning et al., 2018). Lastly, analysis of the surface electrostatics reveals that both HIV-1 and SIVrcm Vif are highly basic proteins, with SIVrcm Vif having a distinctly larger basic patch than HIV-1 Vif (Figure 1E and 1F). These notable structural differences between SIVrcm and HIV-1 VCBC likely underlie the functionally distinct properties of the Vif proteins from each species, particularly in their ability to antagonize different A3 proteins in a species-specific manner.

SIVcpz Vif and SIVrcm Vif use a common hydrophobic surface to antagonize cpzA3G

Multiple mutagenesis studies have mapped the A3G and A3D binding regions to a subset of residues that cluster on the surface of HIV-1 VCBC (Figure 2A) (Guo et al., 2014; Pery et al., 2009; Russell and Pathak, 2007). Despite this work, it remains unclear how Vif binds A3s or how lentiviral Vifs confer species-specific recognition of their cognate A3G and A3D. Comparison of the HIV-1 and SIVrcm Vif structures revealed that hydrophobic residues critical for A3G antagonism in HIV-1 (40-YRHHY-44 and W70) are well conserved in SIVrcm (42-YVPHF-46 and W74) and SIVcpz (40-YRHHY-44 and W70) (Figures 2B and S2). Therefore, we hypothesized that HIV-1 Vif, SIVcpz Vif, and SIVrcm Vif use a common, hydrophobic surface to engage A3G. As SIVrcm Vif partially counteracts the antiviral effects of cpzA3G (6.4-fold less than SIVcpz Vif, but ~10-fold over background), we mutated hydrophobic residues Y42, F46, and W74 to alanine and tested them in a single-cycle infectivity assay against cpzA3G (Figure 2C, **left**). The Y42A and F46A mutations abolished the ability of SIVrcm Vif to antagonize cpzA3G, and the SIVrcm Vif W74A mutation reduced infectivity ~5-fold compared to SIVrcm Vif. Importantly, these mutations are able to antagonize cpzA3H, indicating that they form fully functional E3 ligases (Figure 2C, **right**). These data demonstrate that SIVrcm Vif utilizes this cluster of hydrophobic residues to engage A3G in a manner that is similarly observed for hominid primate Vifs, and subsequent adaptations needed for efficient antagonism of cpzA3G are likely within proximity of this hydrophobic patch.

SIVrcm Vif Y86 is the primary molecular determinant that governs species-specific antagonism of hominid A3G

To identify adaptations that allowed SIVrcm Vif to gain the ability to degrade cpzA3G, we focused our efforts on residues immediately after HIV-1 Vif W79 (W82 in SIVrcm Vif) as they are 1) in a loop (Loop5) that allows for a high degree of flexibility, 2) are evolutionarily less restricted since they contribute little to the protein fold, and 3) positioned adjacent to the F-box 1 and 2 binding surfaces on HIV-1 Vif (human A3D binding regions) as well as the conserved hydrophobic residues involved in SIVrcm Vif-mediated antagonism of cpzA3G (Figure 3A). Thus, SIVrcm Vif residues 83-LGTY-86 were swapped with the corresponding SIVcpz Vif residues (HLGH) (Figure 3A, SIVrcm Vif L5swap). Strikingly, the resulting construct was able to rescue infection in the presence of cpzA3G (41% rescue versus 9% for SIVrcm Vif or 57% for SIVcpz Vif) (Figure 3B). Moreover, we further narrowed down this adaptation to SIVrcm Vif Y86H, as this single amino acid change was sufficient to restore infectivity to the same level as the SIVrcm Vif L5swap (Figure 3B). Viral packaging assays confirmed that SIVcpz Vif, and to a slightly lesser extent SIVrcm Vif L5swap and SIVrcm Vif Y86H decreased the levels of cpzA3G in both the cell and virion (Figures 3C and S3). In addition to cpzA3G, the SIVrcm Vif Y86H mutation is sufficient to allow SIVrcm Vif to antagonize huA3G (Figure 3D). Thus, a single amino acid change in SIVrcm Vif is sufficient to confer specificity for hominid A3G.

In order to characterize the diversity of Loop5 residues, we compared the SIVrcm Vif residues 82–87 with corresponding residues from SIVcpz and HIV-1 Vifs, as well as SIVagm.ver Vif as the ability of this Vif to antagonize A3Gs differing at positions 128 and 130 have been previously studied (Compton and Emerman, 2013; Compton et al., 2012). To do this we threaded the SIVagm.ver and SIVcpz Vif sequences onto the SIVrcm and HIV-1 Vif structure, respectively, and overlaid the residues of each of these Vifs with SIVrcm Vif (Figure 4 A–D). The amino acids within this region of SIVrcm and SIVagm.ver Vifs are highly similar, which is consistent with these Vifs antagonizing A3Gs containing K128 and D130. Likewise, SIVcpz and HIV-1 Vif are more similar to each other, and these Vif proteins are able to antagonize A3Gs containing D128 and D130. To further distinguish the role of Loop5 residues in determining A3G selectivity, we generated logo plots of this region for SIV Vifs that infect monkeys with a K128/D130 A3G sequence and SIV/HIV Vifs that infect hominid primates (SIVcpz and HIV-1) (Figure 4 E–G). These analyses reveal that there is a strong preference for Y86 in SIV Vifs that antagonize A3Gs containing K128, with the histidine at this position coming solely from SIVagm.gri Vif (Figure 4E). Intriguingly, SIVagm.gri Vif can antagonize A3Gs with either an aspartic acid or glutamic acid at position 128 (Compton et al., 2012). SIVcpz Vifs show a preference for histidine at this same position (H83, Figure 4F) and antagonizes A3Gs containing D128, indicating that a histidine at this position may broaden Vif specificity for A3G mutations at residues 128.

HIV-1 Vif proteins can also accommodate a histidine at position 83, but show a preference for a glutamine, suggesting additional diversification may have occurred within Vif once it entered hominid primates (Figure 4G). To determine if SIVrcm Vif harboring a Y86Q mutation would also gain the ability to antagonize hominid primate A3G, we tested this mutant in a single-cycle infectivity assay. The resulting mutation was able to rescue

infection in the presence of both cpzA3G and huA3G (Figure 4H). Thus, both Y86H and Y86Q are adaptive changes SIVrcm Vif that confer activity against hominid A3G.

Previous studies have determined that the identity of amino acids 128 and 130 in A3G are important for the species-specificity of Vif (Compton et al., 2012; Russell and Pathak, 2007; Schröfelbauer et al., 2004). As residue 128 is an aspartic acid (D128) in human and chimpanzee A3G and a lysine (K128) in rcmA3G, we wanted to directly test the hypothesis that SIVrcm Vif adapted at position Y86 to accommodate this change in huA3G (huA3G-D128K). We observed that SIVrcm Vif antagonizes huA3G-D128K better than wild-type huA3G (14.4% from 3.6%, p=0.0109), indicating a preference of SIVrcm Vif to huA3G K128. Conversely, mutating SIVrcm Vif Y86 to either H or Q decreases antagonism of huA3G-D128K (similar to the low antagonism seen by SIVrcm Vif against wild-type huA3G) and switches the preference to wild-type huA3G (Figure 4I). Intriguingly, all of these SIVrcm Vif constructs retain the ability to antagonize rcmA3G. This not only indicates that these mutations are able to form functional E3 ligases, but also suggests that additional species specificity factors contribute to A3G recognition as rcmA3G and huA3G-D128K are identical in the well-studied Vif binding region of A3G (128-KPD-130). Together, these data point to the identity of SIVrcm Vif residue 86 (or the corresponding residues in other Vifs) as a dynamic specificity determinant that enables Vif adaptation for A3 antagonism.

Residues in the overprinted C-terminus of Vif are needed for A3F and A3H antagonism, but dispensable for A3D and A3G antagonism

The unique CTD of SIVcpz Vif that was reconstructed during the "overprinting" event spans from the BC-box to the C-terminus, and the only structural element within this region is the α5 helix. The structure of SIVrcm Vif revealed that the α5 helix is positioned at the C-terminus of the protein, and therefore lacks a stretch of residues corresponding to a critical A3F-binding region in HIV-1 known as F-box 3. HIV-1 Vif uses multiple binding surfaces, known as F-box 1, 2, and 3, to engage A3F (Figure 5A). Mutagenesis studies have shown that HIV-1 F-box 1 and 2 residues (D14/R15 and W79, respectively) are also critical for A3D antagonism, suggesting that A3D engages HIV-1 VCBC in a binding mode similar to A3F (Zhang et al., 2008). In contrast to the weak antagonism of SIVrcm Vif against cpzA3G (~10% rescue of infectivity), SIVrcm Vif is unable to antagonize cpzA3D (Figure 5B) (Etienne et al., 2013). Given the functional importance of F-box 3 in A3F antagonism in hominid primates, we wanted to determine if the lack of F-box 3 in SIVrcm could explain its inability to antagonize cpzA3D.

To our knowledge, F-box 3 has never been shown to be involved in degrading hominid primate A3D. Therefore, we initially asked if SIVcpz Vif F-box 3 was required for A3D antagonism. A single-cycle infectivity assay was used to assess the ability of SIVcpz Vif and a SIVcpz Vif truncation lacking F-box 3 (cpzVif F3) to counteract cpzA3F/G/D/H (Figure 5C). We also included A3H in our assays as the role of F-box 3 has never been tested for the A3H antagonism. Similar to previous studies, SIVcpz Vif F-box 3 was required to counteract A3F, but dispensable for A3G (Dang et al., 2010; Nakashima et al., 2016). In contrast to the previous notion that A3D binds VCBC in an A3F-like manner, SIVcpz Vif F-box 3 was not required for A3D antagonism; therefore, demonstrating that SIVcpz VCBC,

and likely HIV-1 VCBC, use overlapping, but distinct binding modes to engage A3F and A3D. Viral packaging assays confirmed that packaging of cpzA3F is decreased in the presence of SIVcpz Vif but is largely rescued in the presence of SIVcpz Vif F3 (Figure 5D), confirming that observed differences in antiviral activity correlate to changes in A3 viral packaging. Surprisingly, deletion of F-box 3 impaired SIVcpz Vif's ability to antagonize A3H, thus establishing a functional role of the Vif CTD in A3H antagonism. These data establish that residues after the α5 helix did not contribute to the adaptation events needed to counteract cpzA3G or cpzA3D, but likely played a role in maintaining the ability of SIVcpz to antagonize hominid A3F and A3H.

Discussion

The crystal structure of the SIVrcm VCBC complex illuminated an evolutionary step preceding the cross-species transmission of SIV into chimpanzee populations. Our structure-function studies enabled us to assess the contributions of various Vif adaptations in their ability to antagonize cpzA3G and to ultimately pinpoint specific Vif adaptations that played a critical role in overcoming at least one of the species-specific barriers imposed by hominid primate A3s. Structural analysis of SIVrcm Vif identified both similarities and key differences between the molecular assemblies of the SIVrcm Vif and HIV-1 VCBC complexes. We observed that HIV-1 Vif and SIVrcm Vif adopt the same overall protein fold and that the major structural differences, particularly those of functional relevance, were located within loop regions. Differences in the sequence and length of these regions precluded our ability to obtain accurate alignments or homology models of SIVrcm Vif, and only by solving the structure were we able to determine the structural consequences of the overprinting event that produced SIVcpz Vif. The importance of CBFβ in stabilizing the fold of Vif proteins in both the SIVrcm VCBC and HIV-1 VCBC complexes suggests that CBFβ plays an essential scaffolding role in all primate Vifs (Hultquist et al., 2012; Kane et al., 2015). Based on the high degree of structural similarity between SIVrcm and HIV VCBC, and on the observation that all primate Vifs require CBFβ to antagonize A3s, we anticipate that primate Vifs share a common protein fold. This finding will facilitate efficient homology modeling of additional lentiviral Vifs to better predict how mutations contribute to zoonotic transmission.

The SIVrcm structure allowed for a detailed comparison of an OWM Vif to HIV-1 Vif and revealed how structural variations in loop regions contribute to the functional differences related to Vif substrate specificity. We used this information to establish that hydrophobic residues implicated in HIV-1 Vif-A3G binding also contribute to SIVrcm Vif-mediated antagonism of A3G. This finding suggests that the hydrophobic Vif-A3G binding mode is evolutionarily conserved. On the periphery of this hydrophobic patch, we identified a single amino acid change (SIVrcm Vif Y86H) that confers specificity towards cpzA3G and huA3G. Interestingly, previous studies have implicated residues within this loop region of Vif as important for A3G antagonism (Compton et al., 2012, 2013; Letko et al., 2015). In these studies, the amino acid identity of A3G residues 128 and 130 governed Vif susceptibility. It was determined that SIVagm Vif (African green monkey) evolved *in vivo* to re-establish agmA3G antagonism, and that SIVagm Vif adaptation to an agmA3G haplotype encoding 130H selected for a Y84C mutation within Vif (Compton et al., 2012). Similarly,

in vitro evolution studies with HIV-1 Vif and an A3G mutated at position 130 (huA3G 130R), revealed that adaptation to this mutant A3G selected for a G82D mutation within Vif (Letko et al., 2015). It is important to note that these studies specifically looked at Vif adaptations to changes in position 130 of A3G. In the work presented here, that is not the case as the amino acid identity of residue 130 is the same for huA3G, cpzA3G, and rcmA3G.

Here we show that SIVrcm Vif adapted at position Y86 to gain the ability to antagonize hominid primate A3Gs and to at least in part accommodate a change in A3G at position 128. As histidine or glutamine at SIVrcm Vif position 86 are both sufficient to antagonize hominid primate A3G, it is worth noting that the tyrosine to histidine mutation observed between SIVrcm and SIVcpz Vifs requires only a single base substitution and the tyrosine to glutamine mutation observed between SIVrcm and HIV-1 Vifs requires two substitutions, yet glutamine could arise from tyrosine via histidine base mutation. Therefore, these data suggest that the adaptation to histidine arose initially to enter chimpanzee population and that this adaptation was sufficient for transmission into human populations. However, once in the human population additional evolutionary pressures resulted in a subsequent base substitution yielding a glutamine at this position in Vif.

Several previous lines of evidence suggested that A3D bound Vif in a manner similar to A3F. Specifically, the fact that HIV-1 Vif uses F-box 1 and 2 to antagonize both huA3F and huA3D (Zhang et al., 2008) and that analogous residues in A3F and A3D are involved in the HIV-1 Vif-binding (Kitamura et al., 2012). However, we determined that SIVcpz Vif does not require F-box 3 to counteract cpzA3D. By establishing that F-box 3 is dispensable for cpzA3D antagonism, our data indicate that SIVcpz Vif, and likely HIV-1 Vif, uses distinct binding modes to antagonize A3F and A3D. Despite our efforts and the proximity of our mutations to known HIV-1 Vif residues involved in A3D antagonism, we were unable to identify adaptations that restored SIVrcm Vif's ability to antagonize cpzA3D. A major limitation was the fact that we based our hypotheses for A3D antagonism off of available data from HIV-1 studies with huA3D and huA3F. As SIVrcm Vif lacks F-box 3, yet retains the ability to antagonize cpzA3F, it raised the question: how SIVrcm Vif binds cpzA3F without this critical A3F binding motif? Without more mechanistic information on the SIVrcm Vif-cpzA3F interaction, we were unable to delineate critical resides that allow SIVrcm Vif to differentiate between cpzA3F and cpzA3D, as well as identify determinants that allow SIVcpz Vif, but not SIVrcm Vif, to degrade cpzA3D. The molecular basis for the differential recognition of A3F and A3D by Vif is currently unclear and will be addressed in future studies.

Our findings highlight the functional importance of loops in Vif in the co-evolution of Vif-A3G interactions, specifically Loop5. Given the strong likelihood that primate Vif proteins have the same conserved protein fold, unstructured loops would be evolutionarily important for Vif to adapt to new A3s. Relying on loop residues for the molecular "arms-race" with A3s would provide an advantage for Vif as they are evolutionarily less restricted and contribute little to the protein fold or stability, and would have a high degree of flexibility. This coupled with the fact that Vif often uses multiple, discontinuous surfaces to engage A3s, would potentially allow Vif to evolve rapidly to different A3 substrates. For example, if

one A3 binding surface was destabilized, it would weaken, but not abolish, the Vif-A3 interaction and the remaining binding surfaces, if located in loops, would be able to sample a larger mutational space to find an optimal compensatory change to restore the interaction. This presents an attractive model for how Vif could use conserved protein interacting surfaces, such as the hydrophobic residues used in the Vif-A3G interaction, as well as evolutionary dynamic specificity determinants to overcome A3 species-specificity.

In conclusion, we have structurally and functionally characterized the SIVrcm Vif substrate receptor complex to reveal adaptations that occurred during the cross-species lentiviral transmission event that led to SIVcpz. This work advances our understanding of the Vif-A3 interactions and reveals insight into the evolutionary requirements for cross-species transmission of SIV into hominid primates that underlie the origins of HIV-1 in humans.

STAR Methods

Lead Contact and Materials Availability

Further information and requests for resources should be directed to and will be fulfilled by the Lead Contact, John D. Gross (jdqross@cql.ucsf.edu).

Experimental Model and Subject Details

Cell lines—HEK293T and SupTI cells were obtained from ATCC. HEK293T cells were cultured in DMEM, (Gibco, #11965092) supplemented with 10% HyClone Bovine Growth Serum (GE Healthcare, #SH3054103) and 1X Penicillin-Streptomycin (Gibco, #15140122). SupTI cells were cultured in RPMI-1640 (Gibco, #11875093) supplemented with 10% HyClone Fetal Bovine Serum (GE Healthcare, #SH30910.03) and 1X Penicillin-Streptomycin (Gibco, #15140122). Cell lines were cultured at 37°C and 5% CO_2 in a humidified incubator, and were maintained for under two months before returning to a lower-passage frozen stock. Cells were mycoplasma-free and routinely tested for mycoplasma contamination at the Specimen Processing/Research Cell Bank core facility at Fred Hutchinson Cancer Research Center.

HEK293T cells were transfected with *TransIT-LT1* Transfection Reagent (Mirus, #MIR 2304) using the manufacturer's recommended protocol. For infectivity assays, HEK293T cells were seeded at 3.75×10^4 cells/well in 90 μL/well in a 96-well plate directly onto DNA complexes (60 ng pLAI envLuc2 vif, 30 ng APOBEC, and 10 ng L-VSV-G, 10 μL total) for reverse transfection. For viral packaging assays, HEK293T cells were seeded at 3.0×10^5 cells/well in a 6-well plate 24 hours prior to transfection with 1000 ng pLAI envLuc2 vif and 500 ng of APOBEC plasmids, or vector control.

Methods Details

Plasmids—All APOBEC-expressing plasmids were constructed as previously described. N-terminally HA-tagged human APOBEC3G (NM_021822, (OhAinle et al., 2006), and chimpanzee APOBEC3G (AY331715, (Etienne et al., 2013)) and APOBEC3H (GM03448, (OhAinle et al., 2008)) were expressed in pcDNA3.1. Chimpanzee APOBEC3D (JN247642)

and APOBEC3F (XM_525658.2) were cloned with a C-terminal HA-tag into the pCS2 and pcDNA3.1 vectors, respectively (Duggal et al., 2011).

The SIVrcm Vif sequence was derived from SIVrcmCM8081 (HM803689), and the SIVcpz Vif sequence was derived from SIVcpz*Pts*TAN13 (JQ768416), as previously described (Etienne et al., 2013). SIVcpz Vif truncations and all other SIVrcm Vif mutants were generated using standard PCR or by QuikChange Lightning Multi-Site Directed Mutagenesis (Agilent, #210513). The HIV-1-based molecular clone pLAI envLuc2 vif provirus was used for infectivity and packaging assays. For this vector, the HIV-1 LAI backbone was knocked out for *env* through NdeI/StuI digestion, *vif* was deleted using MluI/XbaI, and the firefly luciferase gene was inserted into *nef* (Li et al., 2010). SIVrcm Vif, SIVcpz Vif, and all Vif mutants were ligated into pLAI envLuc2 vif using the MluI/XbaI restriction sites, sequenced, and screened for aberrant recombination prior to transfection.

Protein expression and purification

All constructs were generated by standard PCR and restriction-based cloning methods unless otherwise noted. HiSö-tagged CBFβ/Vif and ELOC/ELOB were co-expressed in *E. coli* from pET-Duet and pCDF-Duet plasmids, respectively. Human CBFβ, ELOB, and ELOC were used for all VCBC complexes. For E. *coli* expression, plasmids were transformed into E. *coli* BL21(DE3) (invitrogen) cells and grown at 37°C to an optical density of 0. 6–0.8 and induced with 0.5 mM iPTG overnight at 18°C Purified VCBC complex was obtained as described previously (Jäger et al., 2011; Kim et al., 2013). Briefly, all proteins were subjected to Ni-NTA affinity purification followed by a heparin column. Size exclusion chromatography was used as the final purification step, and VCBC was stored in 20mM HEPES pH 8, 300 mM NaCl, 10% glycerol, and 1mM DTT (or 2mM TCEP for protein used in crystallization trials).

Crystallization and structure determination

Initial crystallization conditions for SIVrcm VCBC were identified using commercially available crystallization screens (Qiagen JCSG Core 1–4), and in-house optimized native crystals were grown at 20 °C using the hanging-drop vapor diffusion method. 12.2 mg/ml SIVrcm VCBC was diluted in a 1:1 ratio with reservoir solution containing 100 mM MES (pH 6), 6% PEG 6000, 0.25% v/v Dichloromethane (Hampton Additive #93). Crystals were soaked in reservoir solution containing 30% glycerol and vitrified in liquid nitrogen. Diffraction data were collected at Lawrence Berkeley National Laboratory, beamline 8.3.1 at the Advanced Light Source on an ADSC Quantum 315r CCD detector at 100 K (Table 1). One hundred and eighty frames of data were collected with a frame width of 1.0°. Diffraction data were indexed, scaled and merged using HKL-2000 (Otwinowski and Minor, 1997). The structure was solved using molecular replacement with PHASER in the CCP4 suite (McCoy et al., 2007). The SIVrcm Vif sequence was threaded onto the HIV-1 Vif structure (PDB ID 4N9F) using Phyre2 (Kelley et al., 2015), and the resulting SIVrcm Vif model, along with CBFβ, ELOB, and ELOC (from PDB ID 4N9F) were used as the search models for molecular replacement. The SIVrcm VCBC structure was refined using PHENIX (Adams et al., 2010; Liebschner et al2019). Addition of solvent molecules and manual

model building was performed using Coot (Emsley et al., 2010). Final validation was performed using MOLPROBITY server (Chen et al., 2010).

Structural analysis and visualization

All structural figures were prepared using PyMOL version 2.0.7 (http://www.pymol.org/) (Schrodinger, 2015). Electrostatic surfaces were calculated using PDB2PQR & APBS webservers (http://nbcr-222.ucsd.edu/pdb2pqr_2.0.0/) (Baker et al., 2001; Dolinsky et al., 2007), using the AMBER94 forcefield to calculate charges. Electrostatic surfaces were visualized in PyMol using APBS tools 2.1. The Phyre2 server was used to generate structural models for SIVagm.ver Vif and SIVcpz Vif (Kelley et al., 2015). The SIVagm.ver Vif and SIVcpz Vif sequences were threaded onto SIVrcm Vif and HIV-1 Vif (PDBL 4N9F), respectively.

Infectivity assays

Viruses were propagated in HEK293T cells by reverse transfection of the relevant pLAI envLuc2 vif and APOBEC3 plasmids, and L-VSV-G for pseudotyping (Bartz and Vodicka, 1997). Transfected cells were incubated for 48 hours until the viral supernatant was harvested and clarified of cellular debris by centrifugation in a V-bottom plate (1,000×G for 3 min at room temperature). 5 μL of viral supernatant was saved for quantitation of reverse transcriptase (RT) activity for normalization, as previously described (Vermeire et al., 2012). A standard 10 μL of viral supernatant was directly transferred to 96-well plates containing 90 μL of SupT1 cells (3.75×10^4 cells/well) pretreated with 20 μg/mL DEAE-Dextran. SupT1 cells were incubated for 48 hours at 37 °C and 5% CO_2 prior to lysis with 100 μL of Bright-Glo Luciferase Reagent (Promega #E2610). Lysate was then assessed for luciferase activity using a LUMIstar Omega microplate luminometer (BMG Labtech). Raw luciferase values were normalized to 2,000 mU RT activity. Percent infectivity values were calculated relative to no APOBEC3 vector control (where no APOBEC3 was set to 100%).

Viral packaging and western blotting

Transfected cells were incubated at 37 °C and 5% CO_2 for 72 hours prior to harvesting supernatant and cells for western blotting. Viral supernatant was clarified of cell debris via passage through a 0.22 micron filter, and virus was pelleted on a tabletop centrifuge at maximum speed for 1 hour at 4 °C. Virus pellet was resuspended in 30 uL of 4% SDS in PBS, and 10 uL of NuPAGE 4X LDS Sample Buffer (Invitrogen, #NP0007) was added. Producer cells were washed twice with PBS, pelleted, and lysed in 150 uL of 1% SDS lysis buffer (1% SDS, 50 mM Tris-HCl pH 7.5, and 5 mM fresh DTT) by boiling at 95 G for 10 min. Lysate was normalized by protein concentration determined by Pierce BCA Protein Assay Kit (Thermo Scientific, #23225) and 4X LDS Sample Buffer was added. Both cell (5 μg/well) and viral lysate (10 μL/well) were resolved on a NuPAGE 4–12% Bis-Tris Protein Gel (Invitrogen, #NP0336). Western blotting was performed with primary antibodies anti-HA (Proteintech, #51064–2-AP), anti-Lamin B1 (Proteintech, #12987–1-AP), and anti-HIV-1 p24 (NIH AIDS Reagent Program, #3537 (Toohey et al., 1995; Wehrly and Chesebro, 1997)) all at a dilution of 1:2000. Secondary antibodies used were StarBright Blue 520 Goat Anti-Rabbit IgG (BIO-RAD, #12005869) and StarBright Blue 700 Goat Anti-Mouse IgG

(BIO-RAD, #12005866) at a dilution of 1:10,000. Images were processed using Fiji/ImageJ software (Schindelin et al., 2012).

Sequence alignment

All SIV and HIV-1 Vif sequences were obtained from the Los Alamos HIV database (www.hiv.lanl.gov) (Foley et al., 2018). Sequences were aligned using Geneious 11.1.15 (https://www.geneious.com). Logo plots were generated using WebLogo 3 (Crooks et al., 2004). For SIV Vif sequences that antagonize A3G K128, D130, the logo plot was generated using the consensus sequences of SIVver (37), SIVsmm (32), SIVsab (4), SIVrcm (6), SIVmac (4), and SIVdrl (5), and the representative sequences of SIVtan, SIVmne, and SIVgri. For SIVcpz Vif sequences, 23 sequences were used to generate the logo plot. Finally, for HIV-1 Group M Vif, the logo plot was generated using the consensus sequences of clades A (208), B (2,013), C (719), D (68), F (70), G (71), H (11), J (5), and K (2).

Quantification and Statistical Analysis

For infectivity experiments in Figures 2–5, all measurements are reported as the mean and standard deviation of three biological replicates. For densitometry measurements in Figure S3, the data are reported as the standard deviation from the mean of two biological replicates. Statistics were determined by unpaired t test using GraphPad Prism 7.04. P values less than 0.05 were considered statistically significant and were represented in figures as $*P < 0.05$, $**P < 0.01$, and $***P < 0.001$. Statistical parameters are also reported in the figure legends.

Data and Code Availability

Accession codes: Coordinates and structure factors were deposited in the Protein Data Bank with accession codes PDB 6P59 (SIVrcm VCBC).

Supplementary Material

Refer to Web version on PubMed Central for supplementary material.

Acknowledgments

References

Adams PD, Afonine PV, Bunkoczi G, Chen VB, Davis IW, Echols N, Headd JJ, Hung LW, Kapral GJ, Grosse-Kunstleve RW, et al. (2010). PHENIX: a comprehensive Python-based system for macromolecular structure solution. Acta Crystallogr. D. Biol. Crystallogr 66, 213–221. [PubMed: 20124702]

Anderson BD, and Harris RS (2015). Transcriptional regulation of APOBEC3 antiviral immunity through the CBF- /RUNX axis. Sci. Adv 1, e1500296–e1500296. [PubMed: 26601257]

Bailes E, Gao F, Bibollet-Ruche F, Courgnaud V, Peeters M, Marx PA, Hahn BH, and Sharp PM (2003). Hybrid origin of SIV in chimpanzees. Science (80-.). 300, 1713.

Baker NA, Sept D, Joseph S, Holst MJ, and McCammon JA (2001). Electrostatics of nanosystems: application to microtubules and the ribosome. Proc. Natl. Acad. Sci. U. S. A 98, 10037–10041. [PubMed: 11517324]

Ball KA, Chan LM, Stanley DJ, Tierney E, Thapa S, Ta HM, Burton LA, Binning JM, Jacobsen M, and Gross J (2018). Conformational dynamics of the HIV Vif protein complex. BioRxiv 483099.

Bartz SR, and Vodicka MA (1997). Production of High-Titer Human Immunodeficiency Virus Type 1 Pseudotyped with Vesicular Stomatitis Virus Glycoprotein. Methods 12, 337–342. [PubMed: 9245614]

Binning JM, Smith AM, Hultquist JF, Craik CS, Caretta Cartozo N, Campbell MG, Burton L, La Greca F, McGregor MJ, Ta HM, et al. (2018). Fab-based inhibitors reveal ubiquitin independent functions for HIV Vif neutralization of APOBEC3 restriction factors. PLoS Pathog. 14.

Bogerd HP, Doehle BP, Wiegand HL, and Cullen BR (2004). A single amino acid difference in the host APOBEC3G protein controls the primate species specificity of HIV type 1 virion infectivity factor. Proc. Natl. Acad. Sci. U. S. A 101, 3770–3774. [PubMed: 14999100]

Chen VB, Arendall WB, Headd JJ, Keedy DA, Immormino RM, Kapral GJ, Murray LW, Richardson JS, Richardson DC, and Richardson DC (2010). MolProbity: all-atom structure validation for macromolecular crystallography. Acta Crystallogr. D. Biol. Crystallogr 66, 12–21. [PubMed: 20057044]

Compton AA, and Emerman M (2013). Convergence and Divergence in the Evolution of the APOBEC3G-Vif Interaction Reveal Ancient Origins of Simian Immunodeficiency Viruses. PLoS Pathog. 9, e1003135. [PubMed: 23359341]

Compton AA, Hirsch VM, and Emerman M (2012). The host restriction factor APOBEC3G and retroviral Vif protein coevolve due to ongoing genetic conflict. Cell Host Microbe 11, 91–98. [PubMed: 22264516]

Compton AA, Malik HS, and Emerman M (2013). Host gene evolution traces the evolutionary history of ancient primate lentiviruses. Philos. Trans. R. Soc. B Biol. Sci 368, 20120496.

Crooks GE, Hon G, Chandonia J-M, and Brenner SE (2004). WebLogo: A Sequence Logo Generator. Genome Res. 14, 1188. [PubMed: 15173120]

Dang Y, Davis RW, York IA, and Zheng YH (2010). Identification of 81LGxGxxIxW89 and 171EDRW174 Domains from Human Immunodeficiency Virus Type 1 Vif That Regulate APOBEC3G and APOBEC3F Neutralizing Activity. J. Virol 84, 5741–5750. [PubMed: 20335268]

Daugherty MD, and Malik HS (2012). Rules of Engagement: Molecular Insights from Host-Virus Arms Races. Annu. Rev. Genet 46, 677–700. [PubMed: 23145935]

Desrosiers RC, Lifson JD, Gibbs JS, Czajak SC, Howe AY, Arthur LO, and Johnson RP (1998). Identification of highly attenuated mutants of simian immunodeficiency virus. J. Virol 72, 1431–1437. [PubMed: 9445045]

Dolinsky TJ, Czodrowski P, Li H, Nielsen JE, Jensen JH, Klebe G, and Baker NA (2007). PDB2PQR: expanding and upgrading automated preparation of biomolecular structures for molecular simulations. Nucleic Acids Res. 35, W522–5. [PubMed: 17488841]

Duggal NK, Malik HS, and Emerman M (2011). The Breadth of Antiviral Activity of Apobec3DE in Chimpanzees Has Been Driven by Positive Selection. J. Virol 85, 11361–11371. [PubMed: 21835794]

Emsley P, Lohkamp B, Scott WG, and Cowtan K (2010). Features and development of Coot. Acta Crystallogr. D. Biol. Crystallogr. 66, 486–501.

Etienne L, Hahn BH, Sharp PM, Matsen FA, and Emerman M (2013). Gene loss and adaptation to hominids underlie the ancient origin of HIV-1. Cell Host Microbe 14, 85–92. [PubMed: 23870316]

Etienne L, Bibollet-Ruche F, Sudmant PH, Wu LI, Hahn BH, and Emerman M (2015). The Role of the Antiviral APOBEC3 Gene Family in Protecting Chimpanzees against Lentiviruses from Monkeys. PLoS Pathog. 11.

Foley B, Leitner T, Apetrei C, Hahn BH, Mizrachi I, Mullins JI, Rambaut A, Wolinsky S, and Korber BT (2018). HIV Sequence Compendium 2018. Theor. Biol. Biophys. Group, Los Alamos Natl. Lab NM LA-UR 18–25673.

Gifford RJ (2012). Viral evolution in deep time: Lentiviruses and mammals. Trends Genet. 28, 89–100. [PubMed: 22197521]

Guo Y, Dong L, Qiu X, Wang Y, Zhang B, Liu H, Yu Y, Zang Y, Yang M, and Huang Z (2014). Structural basis for hijacking CBF-β and CUL5 E3 ligase complex by HIV-1 Vif. Nature 505, 229–233. [PubMed: 24402281]

Harris RS, and Dudley JP (2015). APOBECs and virus restriction. Virology 479–480, 131–145.

Hultquist JF, Lengyel JA, Refsland EW, LaRue RS, Lackey L, Brown WL, and Harris RS (2011). Human and Rhesus APOBEC3D, APOBEC3F, APOBEC3G, and APOBEC3H Demonstrate Conserved Capacity To Restrict Vif-Deficient HIV-1. J. Virol. 85, 11220–11234. [PubMed: 21835787]

Hultquist JF, Binka M, Larue RS, Simon V, and Harris RS (2012). Vif Proteins of Human an Simian Immunodeficiency Viruses Require Cellular CBF To Degrade APOBEC3 Restriction Factors.

Jäger S, Kim DY, Hultquist JF, Shindo K, LaRue RS, Kwon E, Li M, Anderson BD, Yen L, Stanley D, et al. (2011). Vif hijacks CBF-β to degrade APOBEC3G and promote HIV-1 infection Nature 481, 371. [PubMed: 22190037]

Kane JR, Stanley DJ, Hultquist JF, Johnson JR, Mietrach N, Binning JM, Jónsson SR, Barelier S, Newton BW, Johnson TL, et al. (2015). Lineage-Specific Viral Hijacking of Non-canonical E3Ubiquitin Ligase Cofactors in the Evolution of Vif Anti-APOBEC3 Activity. Cell Rep. 11, 1236–1250. [PubMed: 25981045]

Kelley LA, Mezulis S, Yates CM, Wass MN, and Sternberg MJE (2015). The Phyre2 web portal for protein modeling, prediction and analysis. Nat. Protoc. 10, 845–858. [PubMed: 25950237]

Kim DY, Kwon E, Hartley PD, Crosby DC, Mann S, Krogan NJ, and Gross JD (2013). CBFβ Stabilizes HIV Vif to Counteract APOBEC3 at the Expense of RUNX1 Target Gene Expression. Mol. Cell 49, 632–644. [PubMed: 23333304]

Kitamura S, Ode H, Nakashima M, Imahashi M, Naganawa Y, Kurosawa T, Yokomaku Y, Yamane T, Watanabe N, Suzuki A, et al. (2012). The APOBEC3C crystal structure and the interface for HIV-1 Vif binding. Nat. Struct. Mol. Biol 19, 1005–1011. [PubMed: 23001005]

Letko M, Booiman T, Kootstra N, Simon V, and Ooms M (2015). Identification of the HIV-1 Vif and Human APOBEC3G Protein Interface. Cell Rep. 13, 1789–1799. [PubMed: 26628364]

Li MMH, Wu LI, and Emerman M (2010). The Range of Human APOBEC3H Sensitivity to Lentiviral Vif Proteins †. J. Virol 84, 88–95. [PubMed: 19828612]

Liebschner D, Afonine PV, Baker ML, Bunkoczi G, Chen VB, Croll TI, Hintze B, Hung L-W, Jain S, McCoy AJ, et al. (2019). Macromolecular structure determination using X-rays, neutrons and electrons: recent developments in Phenix. Acta Crystallogr. Sect. D Struct. Biol 75, 861–877. [PubMed: 31588918]

McCoy AJ, Grosse-Kunstleve RW, Adams PD, Winn MD, Storoni LC, and Read RJ (2007). Phaser crystallographic software. J. Appl. Crystallogr 40, 658–674. [PubMed: 19461840]

Nakashima M, Ode H, Kawamura T, Kitamura S, Naganawa Y, Awazu H, Tsuzuki S, Matsuoka K, Nemoto M, Hachiya A, et al. (2016). Structural Insights into HIV-1 Vif-APOBEC3F Interaction. J. Virol 90, 1034–1047. [PubMed: 26537685]

OhAinle M, Kerns JA, Malik HS, and Emerman M (2006). Adaptive Evolution and Antiviral Activity of the Conserved Mammalian Cytidine Deaminase APOBEC3H. J. Virol 80, 3853–3862. [PubMed: 16571802]

OhAinle M, Kerns JA, Li MMH, Malik HS, and Emerman M (2008). Antiretroelement Activity of APOBEC3H Was Lost Twice in Recent Human Evolution. Cell Host Microbe 4, 249–259. [PubMed: 18779051]

Otwinowski Z, and Minor W (1997). Processing of X-ray diffraction data collected in oscillation mode in Methods in Enzymology.

Pery E, Rajendran KS, Brazier AJ, and Gabuzda D (2009). Regulation of APOBEC3 proteins by a novel YXXL motif in human immunodeficiency virus type 1 Vif and simian immunodeficiency virus SIVagm Vif. J. Virol 83, 2374–2381. [PubMed: 19109396]

Russell RA, and Pathak VK (2007). Identification of two distinct human immunodeficiency virus type 1 Vif determinants critical for interactions with human APOBEC3G and APOBEC3F. J. Virol 81, 8201–8210. [PubMed: 17522216]

Schindelin J, Arganda-Carreras I, Frise E, Kaynig V, Longair M, Pietzsch T, Preibisch S, Rueden C, Saalfeld S, Schmid B, et al. (2012). Fiji: an open-source platform for biological-image analysis. Nat. Methods 9, 676–682. [PubMed: 22743772]

Schrodinger (2015). The PyMOL Molecular Graphics System, Version 2.0.7.

Schröfelbauer B, Chen D, and Landau NR (2004). A single amino acid of APOBEC3G controls its species-specific interaction with virion infectivity factor (Vif). Proc. Natl. Acad. Sci. U. S. A 101, 3927–3932. [PubMed: 14978281]

Sharp PM, and Hahn BH (2011). Origins of HIV and the AIDS pandemic. Cold Spring Harb. Perspect. Med 1, a006841. [PubMed: 22229120]

Sheehy AM, Gaddis NC, Choi JD, and Malim MH (2002). Isolation of a human gene that inhibits HIV-1 infection and is suppressed by the viral Vif protein. Nature 418, 646–650. [PubMed: 12167863]

Toohey K, Wehrly K, Nishio J, Perryman S, and Chesebro B (1995). Human Immunodeficiency Virus Envelope V1 and V2 Regions Influence Replication Efficiency in Macrophages by Affecting Virus Spread. Virology 213, 70–79. [PubMed: 7483281]

Vermeire J, Naessens E, Vanderstraeten H, Landi A, Iannucci V, van Nuffel A, Taghon T, Pizzato M, and Verhasselt B (2012). Quantification of Reverse Transcriptase Activity by Real-Time PCR as a Fast and Accurate Method for Titration of HIV, Lenti- and Retroviral Vectors. PLoS One 7.

Wehrly K, and Chesebro B (1997). p24 antigen capture assay for quantification of human immunodeficiency virus using readily available inexpensive reagents. Methods A Companion to Methods Enzymol. 12, 288–293.

Xu H, Svarovskaia ES, Barr R, Zhang Y, Khan MA, Strebel K, and Pathak VK (2004). A single amino acid substitution in human APOBEC3G antiretroviral enzyme confers resistance to HIV-1 virion infectivity factor-induced depletion. Proc. Natl. Acad. Sci. U. S. A. 101, 5652–5657. [PubMed: 15054139]

Yu XX-F, Yu Y, Liu B, Luo K, Kong W, Mao P, and Yu XX-F (2003). Induction of APOBEC3G ubiquitination and degradation by an HIV-1 Vif-Cul5-SCF complex. Science 302, 1056–1060. [PubMed: 14564014]

Zhang W, Chen G, Niewiadomska AM, Xu R, and Yu XF (2008). Distinct determinants in HIV-1 Vif and human APOBEC3 proteins are required for the suppression of diverse host anti-viral proteins. PLoS One 3.

Zhang W, Du J, Evans SL, Yu Y, and Yu XF (2012). T-cell differentiation factor CBF-β regulates HIV-1 Vif-mediated evasion of host restriction. Nature 481, 376–379.

Zhou X, Evans SL, Han X, Liu Y, and Yu XF (2012). Characterization of the interaction of full-length HIV-1 Vif protein with its key regulator CBFβ and CRL5 E3 ubiquitin ligase components. PLoS One 7, e33495. [PubMed: 22479405]

Highlights

- The SIVrcm Vif APOBEC3 (A3G) substrate receptor complex is crystallize at 2.94 Å

- SIVrcm Vif Y86 is the primary determinant that governs antagonism of hominid A3G

- The hydrophobic Vif-A3G binding mode is evolutionarily conserved.

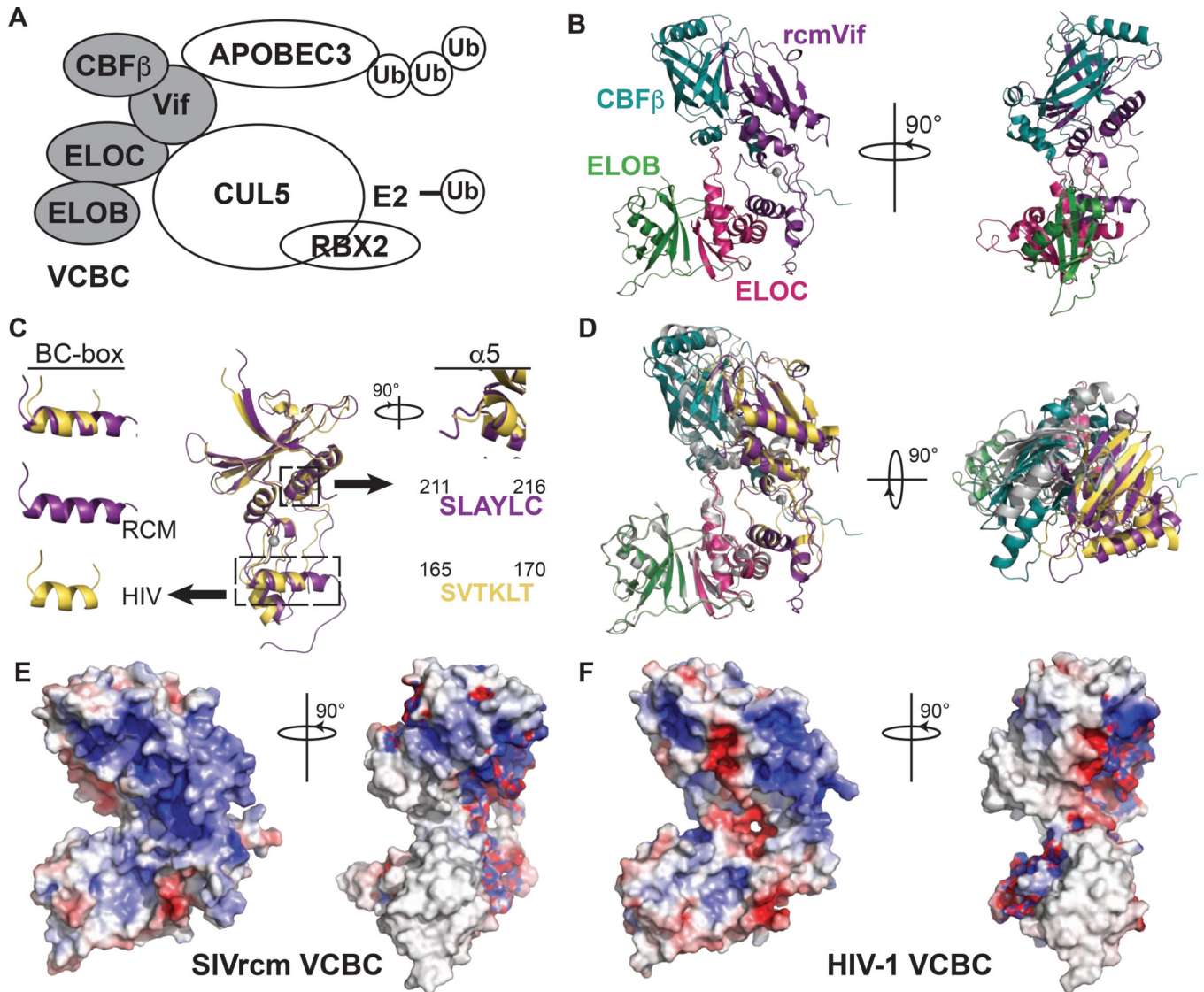- Residues in the Vif CTD are needed to antagonize A3F and A3H, but not A3D and A3G

Figure 1. Crystal structure of SIVrcm VCBC substrate receptor complex.
(A) Schematic representation of the APOBEC3 substrate bound to the Vif E3-ligase with the VCBC components denoted in gray. (B) Ribbon diagram of SIVrcm VCBC complex. Vif, CBFβ, ELOC, and ELOB are colored purple, teal, dark pink, and forest green, respectively. SIVrcm VCBC is colored the same throughout the manuscript. (C) Alignment of SIVrcm Vif and HIV-1 Vif (RMSD = 0.909 Å). Structural differences within the BC-box are shown to the left. The α5 helix, along with the corresponding amino acids for this secondary structural element, are shown to the right. HIV-1 Vif is colored in gold. (D) Structural alignment of the ELOBC subunits from the SIVrcm VCBC structure and the HIV-1 Vif complex structure (PDB 4N9F). HIV-1 VCBC is colored gray with the exception of HIV-1 Vif shown in gold. Electrostatic representation of (E) SIVrcm VCBC and (F) HIV-1 VCBC. Red, white, and blue represent negative, neutral, and positive electrostatic potentials, respectively (range −5 to +5 kT). See also Figure S1–S2.
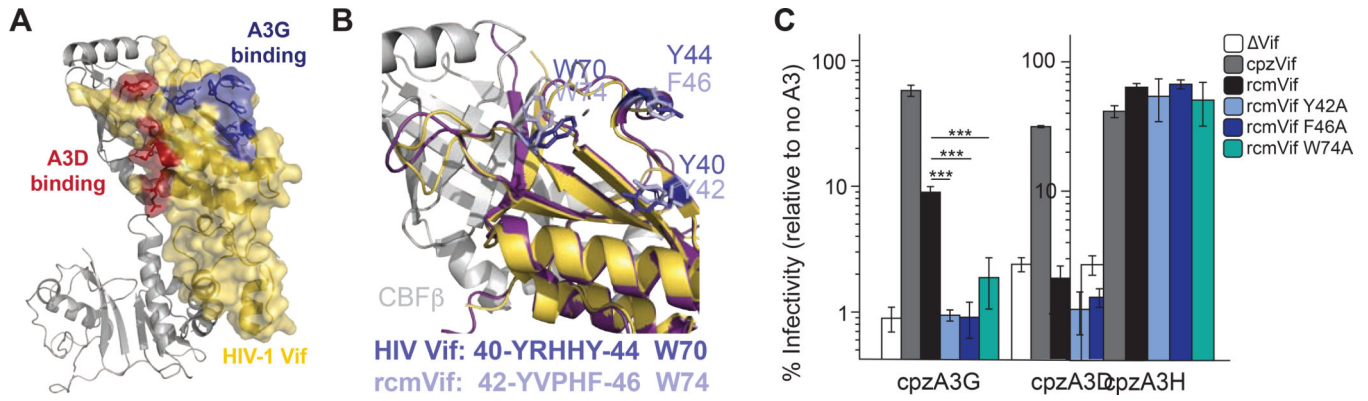
Figure 2. SIVrcm uses a conserved hydrophobic patch to antagonize cpzA3G.
(A) Previously reported A3D (red) and A3G (navy) binding residues mapped onto the surface of HIV-1 Vif (shown in gold). The remaining VCBC components are shown in gray. (B) Hydrophobic A3G binding residues in HIV-1 Vif (Y40, Y44, and W70) and corresponding hydrophobic residues in SIVrcm Vif (Y42, F46, W74). HIV-1 Vif and SIVrcm Vif residues are shown in navy and light blue, respectively. (C) Single-cycle viral infectivity assays performed with virus produced in the presence of cpzA3G and cpzA3H and the absence (ΔVif shown in white) or presence of SIVcpz Vif (grey), SIVrcm Vif (black), SIVrcm Vif Y42A (light blue), SIVrcm Vif F46A (dark blue), or SIVrcm Vif W74A (dark teal). Error bars indicate standard deviation from the mean of three biological replicates. ***$P < 0.001$, unpaired t test.
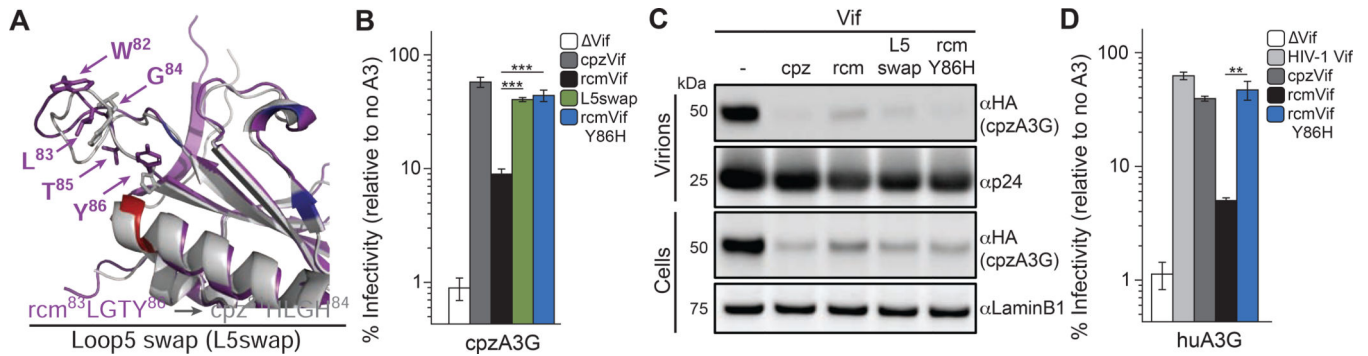
Figure 3. A single amino acid change confers specificity towards human and chimpanzee A3G.
(A) Structural alignment of SIVrcm Vif (purple) and SIVcpz Vif model (gray) with A3G (navy) and A3D (red) binding residues from HIV-1 studies mapped onto the SIVrcm Vif structure. SIVrcm Vif and SIVcpz Vif loop5 amino acid sidechains are shown, with the SIVrcm Vif residues W82, L83, G84, T85, and Y86 highlighted. (B) Single-cycle viral infectivity assays performed with virus produced in the presence of cpzA3G and in the absence (ΔVif shown in white) or presence of SIVcpz Vif (gray), SIVrcm Vif (black), SIVrcm Vif L5swap (green), or SIVrcm Vif Y86H (blue). Error bars indicate standard deviation from the mean of three infection replicates. (C) Immunoblot analysis of cellular cpzA3G levels and packaging into VLPs in the absence and presence of SIVcpz Vif, SIVrcm Vif, SIVrcm Vif L5swap, and SIVrcm Vif Y86H. A3G protein was visualized by WB using anti-HA. Anti-p24 and Anti-LaminB1 were used as loading controls for the VLP and cell fractions, respectively. (D) Single-cycle viral infectivity assays performed with virus produced in the presence of human A3G (huA3G) and the absence (ΔVif shown in white) or presence of HIV-1 LAI Vif (slate), SIVcpz Vif (gray), SIVrcm Vif (black), or SIVrcm Vif Y86H (blue). Error bars indicate standard deviation from the mean of three biological replicates. $**P < 0.01$, $***P < 0.001$, unpaired t test. See also Figure S3.
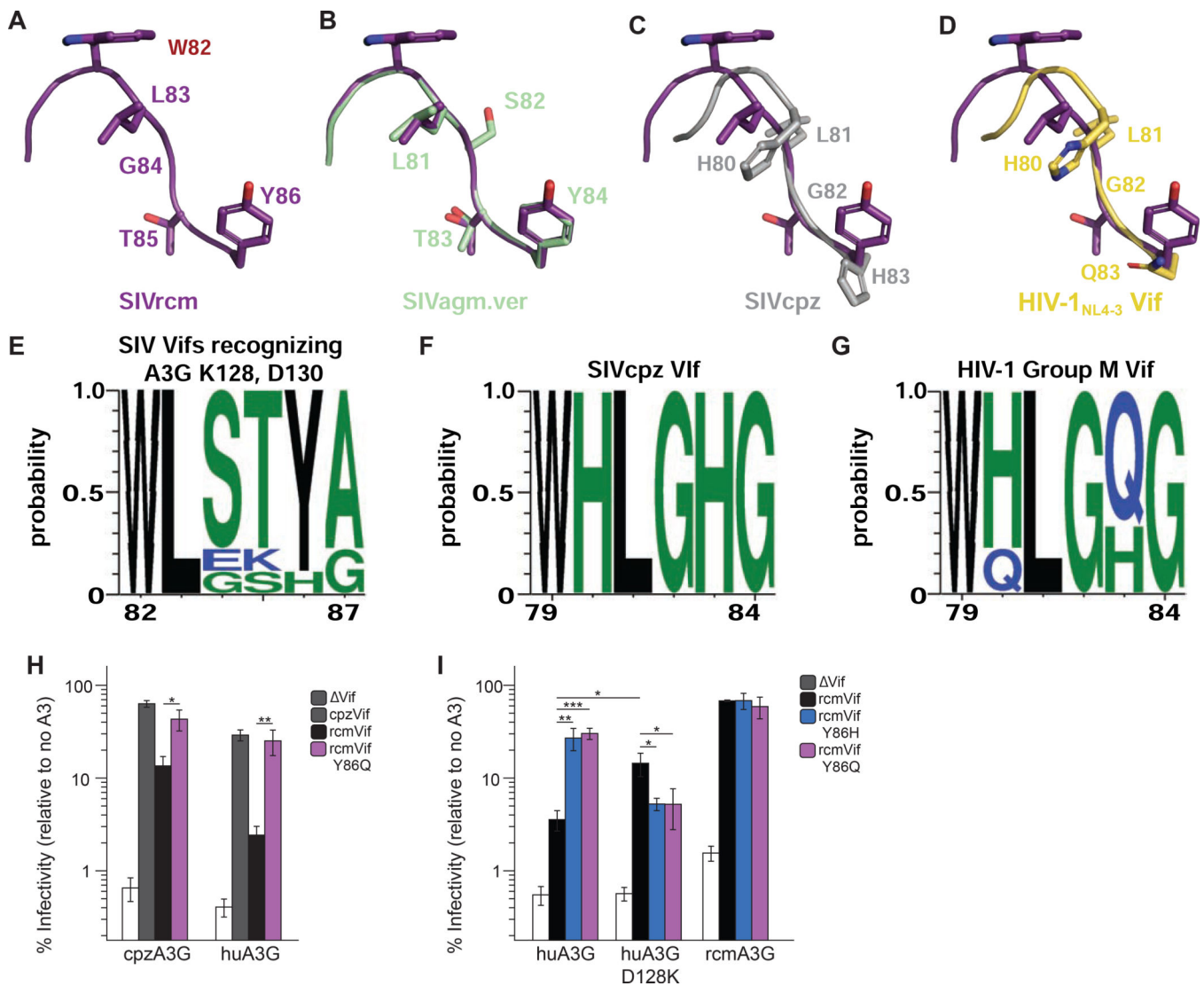
Figure 4. SIVrcm Vif adapted at position Y86 to accommodate changes in hominid A3G.
(A) SIVrcm Vif residues 82–86 alone or aligned with corresponding residues from (B) SIVagm.ver Vif model, (C) SIVcpz Vif model, or (D) HIV-1 Vif. Structural models were generated by threading the SIVcpz and SIVagm.ver Vif sequences onto the HIV-1 and SIVrcm structures, respectively. Logo plots for (E) SIV Vifs that antagonize A3G possessing K128 and D130, (F) SIVcpz Vifs, and (G) HIV-1 Group M Vifs. (H-I) Single-cycle viral infectivity assays performed with virus produced in the presence of indicated A3Gs and in the absence (ΔVif shown in white) or presence of SIVcpz Vif (gray), SIVrcm Vif (black), SIVrcm Vif Y86Q (purple), or SIVrcm Vif Y86H (blue). Error bars indicate standard deviation from the mean of three biological replicates. *$P < 0.05$, **$P < 0.01$, ***$P < 0.001$, unpaired t test.
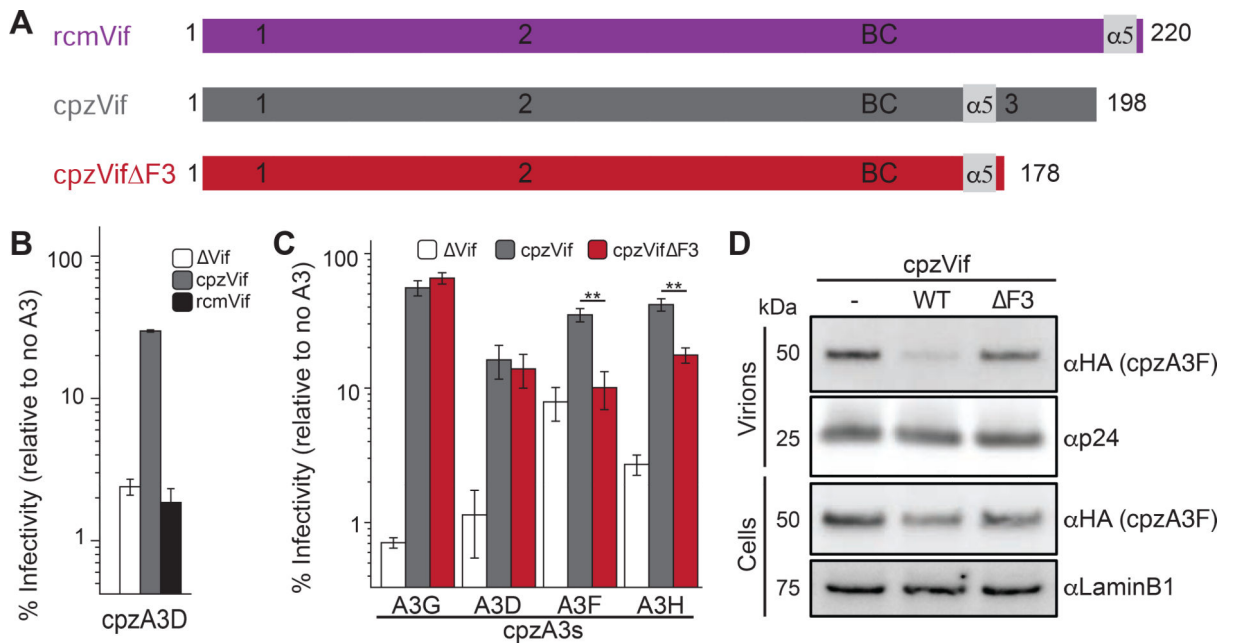
Figure 5. Residues in the overprinted C-terminus of Vif are needed for A3F and A3H antagonism, but dispensable for A3D and A3G antagonism.
(A) Cartoon depiction of Vif constructs used in panels B and C. (B) Single-cycle viral infectivity assays performed with virus produced in the presence of cpzA3D and the absence (ΔVif shown in white) or presence of SIVcpz Vif (gray) or SIVrcm Vif (black). (C) Single-cycle viral infectivity assays performed with virus produced in the presence of cpzA3G, cpzA3D, cpzA3D, and cpzA3H and the absence (ΔVif shown in white) or presence of SIVcpz Vif (gray) or SIVcpz Vif ΔF3 (red). Error bars indicate standard deviation from the mean of three biological replicates. (D) Immunoblot analysis of cellular cpzA3G levels and packaging into VLPs as described in Figure 3C. **$P < 0.05$, unpaired t test.

Table 1.

Data collection and refinement statistics for SIVrcm VCBC, PDB 6P59

Data Collection	
Space group	P 21 21 21
Cell dimensions	
a, b, c (Å)	110.22, 112.49, 125.70
α, β, γ (°)	90.0, 90.0, 90.0
Resolution (Å)	49.12–2.942 (3.047–2.942)
R_{merge} (%)	11.9 (>100)
R_{pim} (%)	5.5 (62.9)
I/σ	12.27 (1.48)
Completeness (%)	98.8 (93)
Redundancy	7.2 (6.5)
CC1/2	0.579
Unique reflections	33445 (3146)
Refinement	
Resolution (Å)	49.12–2.94
No. reflections	33428 (2586)
No. reflections used for R_{free}	1679 (126)
R_{work}	0.2227 (0.3759)
R_{free}	0.2699 (0.4931)
Number of atoms	8925
Protein	8892
Ligand/ion	26
Water	7
Wilson B-factor ($Å^2$)	85.67
Average B-factor ($Å^2$)	103.08
Protein	103.01
Ligands/ion	134.64
Solvent	65.28
R.m.s. deviations	
Bond lengths (Å)	0.003
Bond angles (°)	0.682
Ramachandran plot statistics	
Favored (%)	96.25
Allowed (%)	3.75
Outliers (%)	0
Molprobity clash score	7.59

*
Values in parentheses are for the highest resolution shell.